A&A 463, 187–194 (2007)
DOI: 10.1051/0004-6361:20065915

Astronomy & Astrophysics

Trapping of the H II and photodissociation region in a radially stratified molecular cloud

T. Hosokawa

Division of Theoretical Astrophysics, National Astronomical Observatory, Mitaka, Tokyo 181-8588, Japan
e-mail: hosokawa@th.nao.ac.jp

Received 27 June 2006 / Accepted 16 October 2006

ABSTRACT

Aims. We study the expansion of the ionization and dissociation fronts (DFs) in a radially stratified molecular cloud, whose density distribution is represented as $n(r) \propto r^{-w}$. We focus on cases with $w \leq 1.5$, when the ionization front is "trapped" in the cloud and expands with the preceding shock front. The simultaneous evolution of the outer photodissociation region (PDR) is examined in detail.
Methods. We analytically probe the time evolution of the column densities of the shell and envelope outside the H II region, which are key physical quantities for the shielding of dissociating photons. Next, we perform numerical calculations, and study how the thermal/chemical structure of the outer PDR changes with different density gradients. We apply our numerical model to the Galactic H II region, Sharpless 219 (Sh219).
Results. The time evolution of the column densities of the shell and outer envelope depends on w, and qualitatively changes across $w = 1$. In the cloud with $w < 1$, the shell column density increases as the H II region expands. The DFs are finally trapped in the shell, and the molecular gas gradually accumulates in the shell. The molecular shell and envelope surround the H II region. When $w > 1$, the shell column density initially increases, but then decreases. The column density of the outer envelope also quickly decreases as the H II region increases. It becomes easier for the dissociating photons to penetrate the shell and envelope. The PDR broadly extends around the trapped H II region. A model with $w = 1.5$ successfully explains the observed properties of Sh219. Our model suggests that a density-bounded PDR surrounds the photon-bounded H II region in Sh219.

Key words. stars: early-type – stars: formation – ISM: H II regions – ISM: kinematics and dynamics – ISM: molecules

1. Introduction

H II regions are one of the basic elements of the interstellar medium and have been studied by many groups. The theoretical modeling has advanced from two complementary standpoints. Some studies have modeled the detailed thermal and chemical structure of the static H II region (e.g., Ferland et al. 1998) and photodissociation region (PDR, e.g., Tielens & Hollenbach 1985; Abel et al. 2005). We can compare these models with the observed line-strengths and their ratios to probe the physical state of the target region. Other studies have focused on the dynamical time evolution of the expanding H II region (e.g., Yorke 1986). The density and temperature evolve as the H II region expands and the gas flows across the ionization front (IF). A shock front (SF) sometimes precedes the IF due to high pressure in the H II region. The dynamical evolution is different in different density distributions (Franco et al. 1990, hereafter FTB90). The ionized gas sometimes blows out from the molecular cloud as a "champagne flow" (Tenorio-Tagle 1979).

To assess some recent observations, however, we require up-to-date modeling that includes both the fluid dynamics and consistent thermal/chemical structure (e.g., Ferland 2003; Henney 2006). For example, the "collect and collapse" by the expanding H II region is one of the dynamical triggering processes of star formation (e.g., Elmegreen & Lada 1977; Elmegreen 1998). Recently, high-resolution observations have revealed the detailed structure of the shell around some pc-scale H II regions (Deharveng et al. 2003a, 2005; Zavagno et al. 2006). Dense shell-like structures are traced by the molecular and dust emission around the ionized gas. Young clusters including OB stars are often embedded in fragments of the shell, consistent with the "collect and collapse" scenario. In our previous papers (Hosokawa & Inutsuka 2005, 2006a, hereafter Papers I and II), we focused on the fact that a cold molecular rather than warm neutral shell surrounds the H II region. We have analyzed the dynamical expansion of the H II region, PDR, and the swept-up shell, solving the UV($h\nu > 13.6$ eV) – and FUV($h\nu < 13.6$ eV) – radiative transfer, thermal and chemical processes in a time-dependent hydrodynamics code. Our numerical calculations have shown excellent agreement with some observational properties of a "collect and collapse" candidate. The PDR is quickly trapped in the shell, and a cold and dense molecular shell forms around the H II region in a *homogeneous* ambient medium.

In this paper, we examine how such basic time evolution changes in an *inhomogeneous* ambient medium. Since massive stars form in a dense region in the molecular cloud, such a situation will be more realistic than expansion in a homogeneous medium. Observational features of some H II regions are very different from those of the "collect and collapse" candidates. For example, the Galactic H II region Sharpless 219 (Sh219) has no dense shell. Only a diffuse neutral layer surrounds the ionized gas (Roger & Leahy 1993), although signs of triggering are shown in the adjacent molecular cloud (Deharveng et al. 2003a, 2006). We show that these observational properties are successfully explained by our model, where the H II region and PDR expand in a radially stratified molecular cloud.

The structure of this paper is as follows: in Sect. 2, we briefly discuss the expansion of the H II region and PDR in the radial

density gradient with an analytic treatment. We focus on the time evolution of the column densities of the shell and envelope, which are key physical quantities for the shielding of FUV radiation. In Sect. 3, we investigate the dynamical evolution and trapping of the IF and DFs in the molecular cloud using detailed numerical calculations. We apply our numerical modeling to Sh219 in Sect. 4. In Sects. 5 and 6 we discuss and present our conclusions.

2. Analytic treatment

We study the simultaneous expansion of the H II region and surrounding PDR in an ambient medium presenting a radial density gradient. We adopt a density distribution including a central core and outer envelope,

$$n(r) = \begin{cases} n_{\rm c}, & \text{for } r < R_{\rm c} \\ n_{\rm c}\left(\dfrac{r}{R_{\rm c}}\right)^{-w}, & \text{for } r > R_{\rm c} \end{cases} \quad (1)$$

where $R_{\rm c}$ is the core radius, $n_{\rm c}$ is the core density and $w(>0)$ is the power-law index of the density profile in the outer envelope (FTB90). First, we consider the expansion of the H II region in the analytic approach, following FTB90. The expansion is subject to the balance between the recombination rate in the H II region and supply rate of UV photons by the star. Unless this balance is achieved, the IF quickly propagates in the molecular cloud as an R-type front. It is not until the IF moves out of the cloud that the ionized gas expands due to the pressure gradient (radial "champagne flow"). Once the UV photon supply is balanced by the recombination, on the other hand, the IF decelerates and is "trapped" in the cloud. The IF changes from R-type to D-type, and the SF emerges in front of the IF. FTB90 have shown that this can occur when $w \leq 1.5$. At the moment that the ionization balance is achieved, the radius of the H II region is

$$R_w = R_{\rm st}\left(\frac{R_{\rm st}}{R_{\rm c}}\right)^{2w/(3-2w)}\left[\frac{3-2w}{3} + \frac{2w}{3}\left(\frac{R_{\rm c}}{R_{\rm st}}\right)\right]^{1/(3-2w)} \quad (2)$$

for $w < 1.5$, and

$$R_{1.5} = R_{\rm c}\exp\left[\frac{1}{3}\left[\left(\frac{R_{\rm st}}{R_{\rm c}}\right)^3 - 1\right]\right] \quad (3)$$

for $w = 1.5$, where $R_{\rm st}$ is the Strömgren radius corresponding to the core density. Note that R_w becomes equal to $R_{\rm st}$ with $w = 0$. The subsequent expansion is driven by the high pressure of the H II region. A shell forms around the H II region. A part of the swept-up mass flows into the H II region, and the other part remains in the shell. The total swept-up mass at time t is written as

$$\begin{aligned} M_{\rm sw}(t) &= \frac{4\pi}{3}\rho_{\rm c}R_{\rm c}^3 + \int_{\rm R_c}^{R(t)} \rho_{\rm c}\left(\frac{r}{R_{\rm c}}\right)^{-w} 4\pi r^2\,{\rm d}r \\ &\simeq \frac{4\pi}{3-w}\rho(R)R(t)^3, \end{aligned} \quad (4)$$

where $R(t)$ is the position of the SF, and $\rho(R)$ is the initial mass density at $r = R$ given by Eq. (1). The mass of the ionized hydrogen in the H II region is given by

$$M_{\rm i}(t) = \frac{4\pi}{3}\rho_{\rm i}R_{\rm i}(t)^3, \quad (5)$$

where $R_{\rm i}(t)$ is the position of the IF, and $\rho_{\rm i}(t)$ is the mass density in the H II region at time t. Since the total recombination rate within the H II region always balances the UV-photon number luminosity, the H II density decreases as $\rho_{\rm i} \propto R_{\rm i}^{-3/2}$. Presuming $R(t) \sim R_{\rm i}(t)$, Eqs. (4) and (5) mean that the mass ratio, $M_{\rm sw}(t)/M_{\rm i}(t)$ is proportional to $\rho(R)/\rho_{\rm i}(t) \propto R^{(3-2w)/2}$. Since the SF appears at $R_{\rm i} \sim R_w$, we find

$$\frac{M_{\rm sw}(t)}{M_{\rm i}(t)} \simeq \left[\frac{R(t)}{R_w}\right]^{(3-2w)/2}. \quad (6)$$

Using Eqs. (4)–(6), the H II mass density is written as

$$\rho_{\rm i}(t) \simeq \frac{3}{3-w}\rho(R)\left(\frac{R_w}{R(t)}\right)^{(3-2w)/2}. \quad (7)$$

In this paper, we focus on the structure of the outer PDR as well as the H II region. The PDR structure depends on the efficiency of the shielding of FUV radiation from the central star. Since the FUV radiation is attenuated by the dust absorption and self-shielding effect, the penetration of the PDR is sensitive to the column density of the shell and outer envelope. First, let us evaluate the time evolution of the column density of the shell. Calculating $M_{\rm sw}(t) - M_{\rm i}(t)$ with Eqs. (4), (5) and (7), the mass of the shell at time t is,

$$M_{\rm sh}(t) = \frac{4\pi}{3-w}\rho(R)R(t)^3\left[1 - \left(\frac{R_w}{R(t)}\right)^{(3-2w)/2}\right]. \quad (8)$$

Therefore, the column density of the shell is

$$N_{\rm sh}(t) = \frac{n_{\rm c}R_{\rm c}}{3-w}\left(\frac{R(t)}{R_{\rm c}}\right)^{1-w}\left[1 - \left(\frac{R_w}{R(t)}\right)^{(3-2w)/2}\right]. \quad (9)$$

Equation (9) shows an interesting feature of the time evolution of the shell column density. As the H II region expands, the shell column density increases when $w < 1$, but decreases when $w > 1$. The critical power-law index is $w = 1$, at which the shell column density converges to the constant value of $n_{\rm c}R_{\rm c}/2$. If the density gradient is as steep as $w \sim 1.5$, the column density of the shell is significantly reduced. Supposing a finite size of the cloud, the inner edge of the envelope is the IF and the outer edge is the edge of the cloud. The column density of this outer envelope is

$$\begin{aligned} N_{\rm ev}(t) &= \int_{R(t)}^{R_{\rm out}} n(r)\,{\rm d}r \\ &= \frac{n_{\rm c}R_{\rm c}}{w-1}\left[\left(\frac{R_{\rm c}}{R(t)}\right)^{w-1} - \left(\frac{R_{\rm c}}{R_{\rm out}}\right)^{w-1}\right] \end{aligned} \quad (10)$$

for $w \neq 1$, where $R_{\rm out}$ is the radius of the outer limit of the cloud. Equation (10) shows that the column density of the envelope is mainly determined by $R_{\rm out}$ with $w < 1$, but $R(t)$ with $w > 1$. Therefore, if the density gradient is as steep as $w > 1$, $N_{\rm ev}$ quickly decreases as the H II region expands. Equations (9) and (10) predict that the time evolution of the outer PDR qualitatively changes across $w \sim 1$. The quantitative changes will be significant when the initial column density of the core is about $N_{\rm H} \sim 4$–8×10^{21} cm^{-2}. In a stratified molecular cloud with $w < 1$, the column density of the shell increases as the H II region expands, and the dust absorption becomes significant in the shell. The molecules are shielded from the FUV radiation by the dust, and will accumulate in the shell. This is similar to the evolution in the homogeneous ambient medium studied in Papers I and II. With $w > 1$, on the other hand, the shell column density decreases as the H II region increases. The dust absorption does not take place in the shell, and the PDR extends far beyond the

shell. Furthermore, Eq. (10) shows that the column density of the outer envelope quickly decreases as the H II region expands. Therefore, it becomes easier for the FUV photons to penetrate and photodissociate the outer molecular envelope. In the following sections, we verify our predictions, performing detailed numerical calculations.

3. Numerical calculations

In this section, we present our numerical results calculated with the code developed in Papers I and II (see Paper II for a detailed description), with which we can solve the time evolution of the thermal and chemical structure of the outer PDR as well as of the dynamical evolution of the H II region. The UV/FUV radiative transfer and some chemical rate equations are consistently solved with the hydrodynamics. The dust absorption is included only outside the HII region. We adopt the ambient density distribution given by Eq. (1) with $n_c = 10^5$ cm^{-3}, and the exciting star of 40.9 $M_\odot$. The corresponding stellar UV- and FUV-photon number luminosities are $S_{\rm UV} = 6.0 \times 10^{48}$ s^{-1} and $S_{\rm FUV} = 5.8 \times 10^{48}$ s^{-1} (Diaz-Miller et al. 1998). The Strömgren radius with the adopted n_c and $S_{\rm UV}$ is $R_{\rm st} \sim 2.5 \times 10^{-2}$ pc, and we set the core radius to $R_c = 0.7 R_{\rm st} \sim 1.75 \times 10^{-2}$ pc. The IF and the DFs are initially set at $r = 0.2\,R_c$ and $r = 0.4\,R_c$ respectively.

Figures 1 and 2 present the gas-dynamical evolution with $w = 0.8$ and 1.2 respectively. The dynamical features are similar in both models. When the IF reaches the radius, R_w, the SF appears in front of the IF. FTB90 have provided the approximate equation for the time evolution of the H II radius in this phase,

$$R(t) \simeq R_w \left[1 + \frac{7-2w}{4} \sqrt{\frac{12}{9-4w}} \frac{t}{t_{\rm dyn}} \right]^{4/(7-2w)}, \qquad (11)$$

where $t_{\rm dyn}$ is defined as $R_w/C_{\rm II}$, and $C_{\rm II}$ is the sound speed in the H II region ($T \sim 10^4$ K). Equation (11) still provides a good approximate evolution for our numerical calculations. In both models, the density of the shell is 10–100 times as dense as the region just ahead of the SF. The expansion is faster in the steeper density gradient. The size of the H II region with $w = 1.2$ is about twice as large as that with $w = 0.8$ at the same time, t. The outward velocity within the H II region is higher in a steeper density gradient.

Despite their similar dynamical evolution, the thermal and chemical structures of these model's shells and outer envelopes are very different. The third panels of Figs. 1 and 2 show the temperature profile in each model. With the density gradient of $w = 0.8$ (Fig. 1), the temperature in the outer envelope is kept at $T \sim 10$–30 K, except for just outside the shell. With the steeper density gradient of $w = 1.2$ (Fig. 2), however, the outer envelope is heated up to $T \sim 100$–300 K in the initial 0.1 Myr. Figure 3 shows the chemical structure of the shell and outer envelope with $w = 0.8$ at each time step. The DFs of both H_2 and CO molecules are trapped in the shell by the time $t \sim 0.1$ Myr. The molecular gas gradually accumulates in the outer region of the shell. The outer envelope surrounding the H II region remains molecular. In the model with $w = 1.2$, on the other hand, we can see the different chemical evolution in the upper panel of Fig. 4. While the H_2 DF remains just in front of the SF, the CO DF leaves the SF and quickly travels over the whole cloud. Almost all CO molecules within 10 pc are photodissociated by the time of $t \sim 0.2$ Myr. These clear differences are due to the different evolution of the column densities of the shell and outer envelope, which was predicted in Sect. 2. In the model with

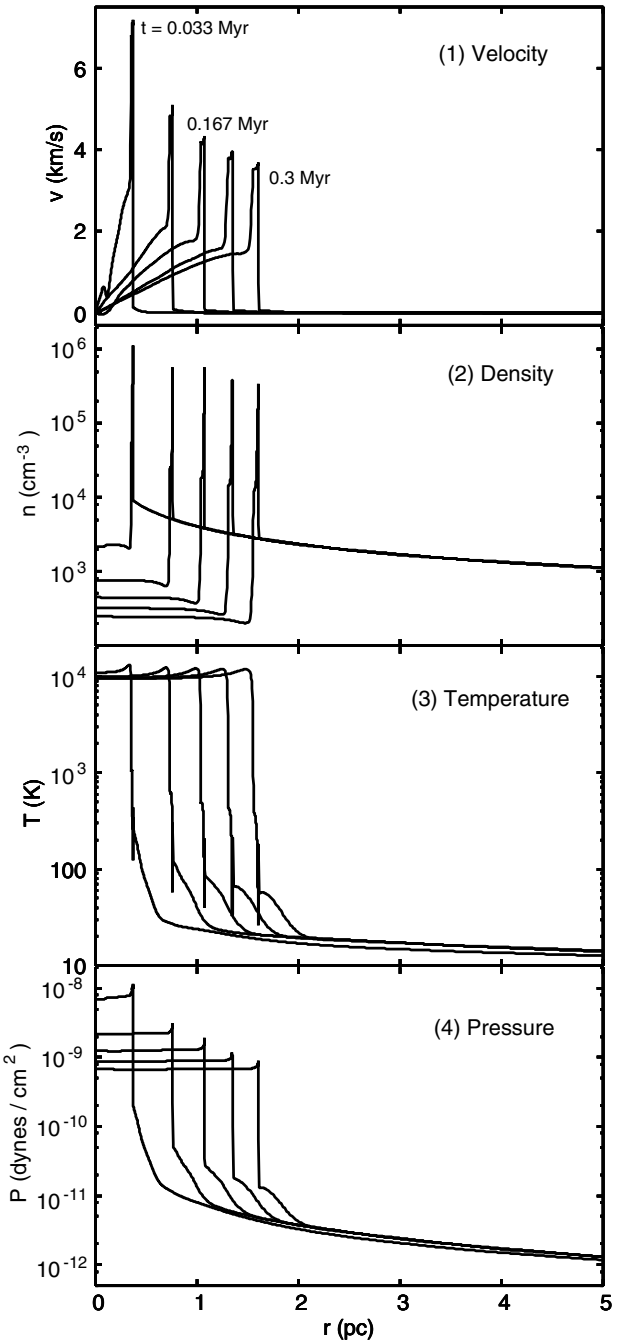

Fig. 1. Gas-dynamical evolution with the density power-law index, $w = 0.8$. In each panel, we present five snapshots at $t = 0.033$, 0.1, 0.167, 0.23, and 0.3 Myr.

$w = 0.8$, the column density of the shell increases as the H II region expands, as the lower panel of Figs. 3 and 5 show. The shell column density attains $N_{\rm sh} \sim 5 \times 10^{21}$ cm^{-2}, which corresponds to $A_V \sim 2.5$, at $t \sim 0.1$ Myr. The significant dust absorption in the shell efficiently blocks FUV photons from the central star. The FUV radiation field in Habing units (Habing 1968) is $G_{\rm FUV} \sim 10^4$ at the IF, but only ~50 at the SF at $t \sim 0.1$ Myr. Consequently, the gas temperature of the outer envelope is as low as $T \sim 10$–30 K, owing to the weak FUV radiation field. Both H_2 and CO molecules are protected against FUV photons by the dust absorption and self-shielding effect, and DFs are easily trapped in the shell. After the DF is engulfed in the shell,

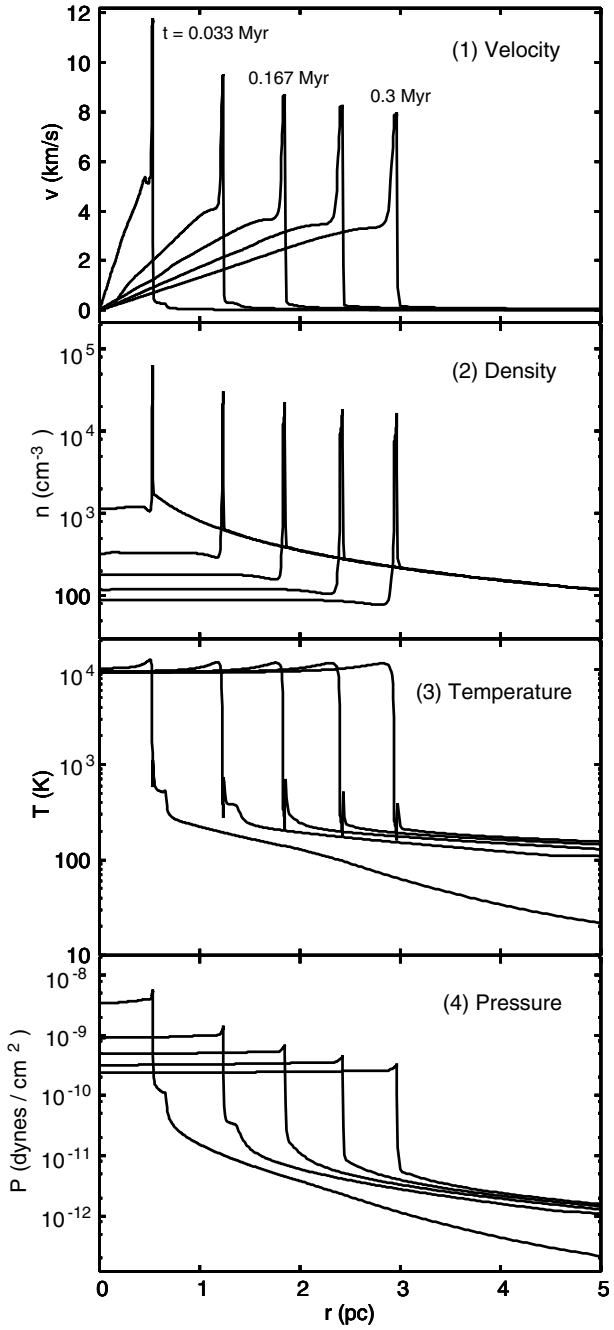

Fig. 2. Same as Fig. 1 but for the density profile with $w = 1.2$.

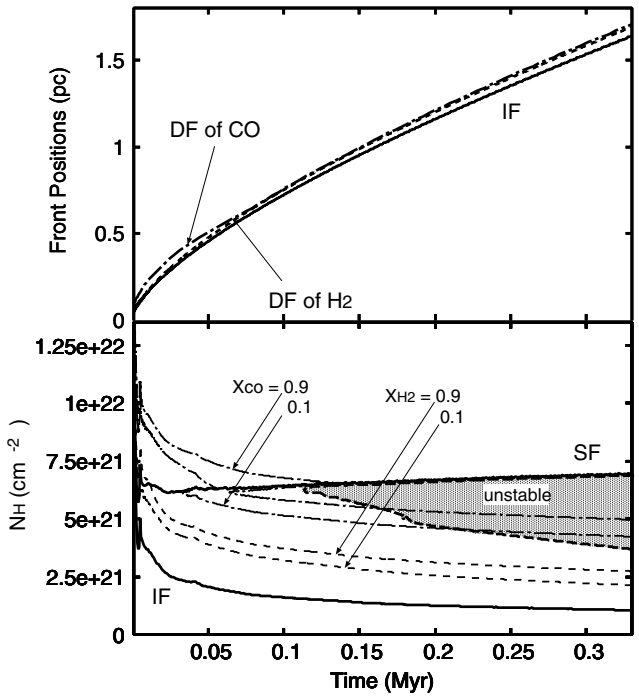

Fig. 3. *Upper panel*: time evolution of some front positions in the model with $w = 0.8$. The solid, broken, and dot-solid lines represent the positions of the IF, DF of the H_2 and CO molecule at each time step. We do not present the position of the SF, which almost traces the position of H_2 DF. *Lower panel*: the time evolution of the column density of each region in the same model. The upper (lower) solid line indicates the position of the SF (IF). Two broken (dot-solid) lines show the position where $x_{H_2}(x_{CO}) = 0.1$ and 0.9. The shaded region denotes the expected gravitationally unstable region, where $t > 1/\sqrt{G\rho}$.

the SF sweeps up the molecular gas in the envelope. The molecular gas accumulates in the shell; this is the same time evolution as in a homogeneous ambient medium (see Papers I and II).

In the steeper density gradient with $w = 1.2$, our model shows the different time evolution of the column density in each region (the lower panel of Figs. 4 and 5). As expected with Eq. (9), the column density of the shell decreases as the H II region expands. Since the shell column density never exceeds 1.0×10^{21} cm^{-3}, the dust absorption in the shell is not sufficient to protect molecules. The self-shielding effect barely enables the gradual accumulation of H_2 molecules in the shell, but the FUV radiation easily photodissociates all CO molecules in the shell. Furthermore, the column density of the outer envelope also quickly decreases following Eq. (10). The column density becomes too low to shield the FUV radiation from the central star by the dust absorption in the envelope. For example, the column density at $r \sim 10$ pc is initially higher than 2.0×10^{22} cm^{-3}, but lower than 4.0×10^{21} cm^{-3} at $t \sim 3$ Myr (Fig. 4). The DF of the CO molecule leaves the SF, and travels over the whole molecular cloud.

In the cloud with a much steeper density gradient, it becomes much easier for the DFs to escape from the dense central region of the cloud. As referred to in Sect. 2, the H II region can be trapped in the cloud with a density stratification of $w \leq 1.5$ (FTB90). Therefore, only the PDR can broadly extend around the trapped H II region with the density profile of $1 \leq w \leq 1.5$. With such a steep density gradient, and if the DFs reach the diffuse outskirts of the cloud, a density-bounded PDR should be observed around the photon-bounded H II region.

4. Application to the Galactic H II region Sharpless 219

4.1. A model with w = 1.5

In this section, we focus on the Galactic H II region, Sharpless 219 (Sh219). Sh219 shows a spherical morphology around a single B0V star; its radius is about 2.2 pc. As mentioned above, Sh219 shows some properties different to those of the "collect and collapse" H II regions. For example, the expanding shell around the H II region is not detected by the molecular emission. Only the half-ring of the PAH emission surrounds the ionized gas (Deharveng et al. 2003a, 2005). Instead of a dense molecular shell, a diffuse atomic layer is widely distributed around

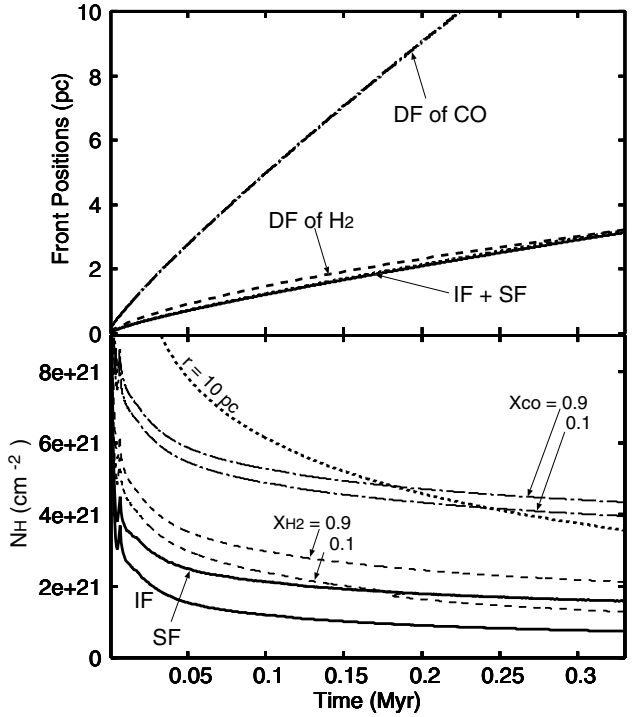

Fig. 4. Same as Fig. 3 but for $w = 1.2$. We plot the position of the SF with a dotted line in the upper panel. Note the differences in scale of the vertical axis from Fig. 3. The dotted line in the lower panel represents the column density at $r \sim 10$ pc. Almost all CO molecules within 10 pc are photodissociated by the time of $t \sim 0.2$ Myr.

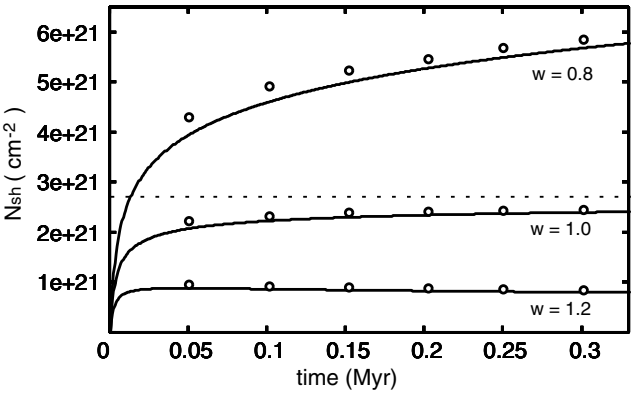

Fig. 5. Time evolution of the column density of the shell with the different density distributions. The three solid lines represent the time evolution expected by Eqs. (9) and (11) with $w = 0.8$, 1.0 and 1.2 *from top to bottom*. The open circles denotes the shell column density calculated every 0.05 Myr in our numerical models. The horizontal dashed line indicates the half column density of the initial homogeneous core, $n_c R_c/2 \sim 2.7 \times 10^{21}$ cm^{-2}.

the H II region, and diffuse far-IR emission has been detected in this region (Roger & Leahy 1993). The radial width of the neutral layer is 2–3 pc. The average number density of the layer is only ∼9 cm^{-3}, which is as low as the density typical of the cold neutral medium, rather than that of the molecular cloud. The number density in the H II region has been estimated as 55 cm^{-3} (Roger & Leahy 1993) and 170 cm^{-3} (Deharveng et al. 2000). Therefore, the ionized gas is much denser than the surrounding neutral layer. These features sharply contrast with those of

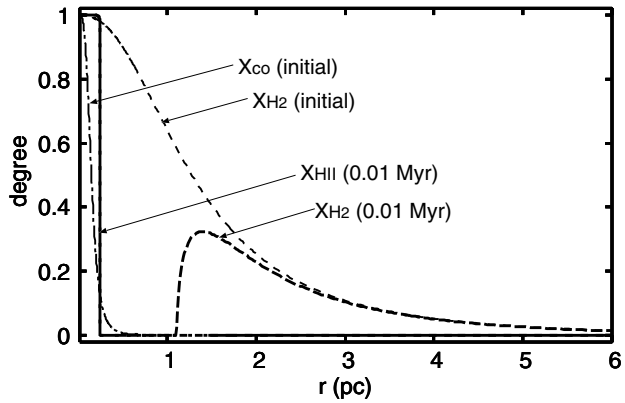

Fig. 6. Snapshots of the chemical structure of our model for Sh219. The thin dot-solid and broken line represent the initial molecular ratios, $X_{\rm CO} \equiv n_{\rm CO}/n_{\rm H,nuc}Z_{\rm C}$ and $X_{\rm H_2} \equiv 2n_{\rm H_2}/n_{\rm H,nuc}$, where $n_{\rm H,nuc}$ is the number density of the hydrogen nuclei. The thick solid and broken line represent the ratios $X_{\rm HII} = n_{\rm H^+}/n_{\rm H,nuc}$ and $X_{\rm H_2}$ at $t = 0.01$ Myr.

a "collect and collapse" H II region, for example, Sharpless 104 (Sh104, Deharveng et al. 2003b). Sh104 is also a pc-scale spherical H II region, but surrounded by a dense molecular shell. The estimated average density and molecular mass of the shell are about 6000 cm^{-3} and 6000 $M_\odot$ respectively. The number density in the H II region is ∼80 cm^{-3}, which is much lower than that of the shell. We have shown that these observational properties of Sh104 are well explained by our model, where the H II region expands in the homogeneous ambient medium of $\sim 10^3$ cm^{-3} (Paper I). In this subsection, we propose an alternative model for Sh219, where the H II region is expanding in a radially stratified molecular cloud.

We adopt the initial density distribution given by Eq. (1) with $w = 1.5$. We adopt a 19 $M_\odot$ star as the central star, and the corresponding UV and FUV luminosities are $S_{\rm UV} = 5.6 \times 10^{47}$ s^{-1} and $S_{\rm FUV} = 1.6 \times 10^{48}$ s^{-1} (Diaz-Miller et al. 1998). The time evolution quantitatively changes with the different parameters of the density and radius of the core. In this section, we present a model with $n_c = 10^5$ cm^{-3} and $R_c = 0.7\, R_{\rm st} \sim 0.07$ pc. The observed neutral layer around Sh219 is so diffuse that we take into account the fact that the FUV background radiation (FBR) penetrates into the cloud. The initial thermal and chemical structure of the cloud are set at the equilibrium determined with the local number density and FUV radiation field. We adopt $G_{\rm FUV} = 1.0$ in Habing units as the fiducial FBR. Note that the strength of the FBR does not affect the chemical/thermal structure outside the H II region when the IF reaches the observed radius of Sh219 (see below). The third panel of Fig. 7 shows that the gas temperature in the outer envelope is initially as high as 100–200 K, due to photoelectric heating by the FBR. The photodissociation by the FBR is significant in the outer diffuse region. More than 90% of H_2 (CO) molecules are initially photodissociated at $r > 3$ pc ($r > 0.3$ pc) (see Fig. 6). Figure 7 shows the gas-dynamical evolution of our model for Sh219. The basic evolution is similar to the models presented in Sect. 3. The IF and preceding SF expand and reach the radius of Sh219, $r \sim 2.2$ pc, at $t \sim 0.1$ Myr. At that time, the number density in the H II region is ∼50 cm^{-3}, and that of the outer layer is ∼10 cm^{-3} at $r \sim 4$ pc. Therefore, the observed density structure of the Sh219 is naturally explained by our model.

The molecular gas in the central dense region is quickly destroyed by the FUV radiation from the central star. H_2 molecules

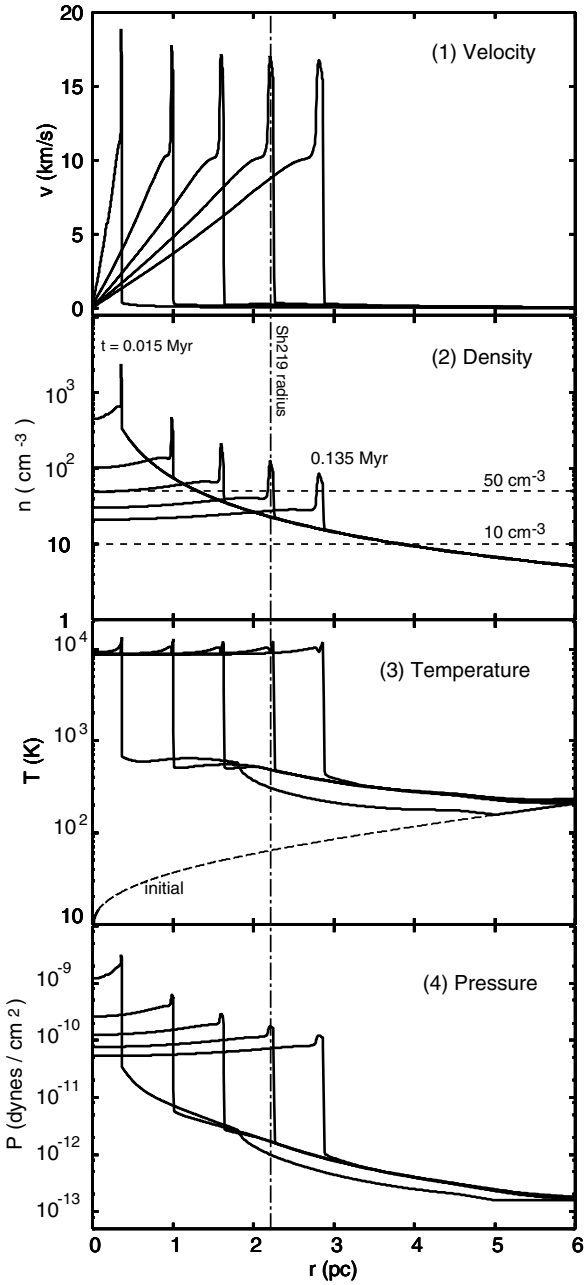

Fig. 7. Gas-dynamical evolution of our model for Sh219. The adopted power-law index of the density profile is $w = 1.5$. We present five snapshots at the time of $t = 0.015$, 0.045, 0.075, 0.105, and 0.135 Myr in each panel. The vertical dot-solid line indicates the observed radius of Sh219, ∼2.2 pc.

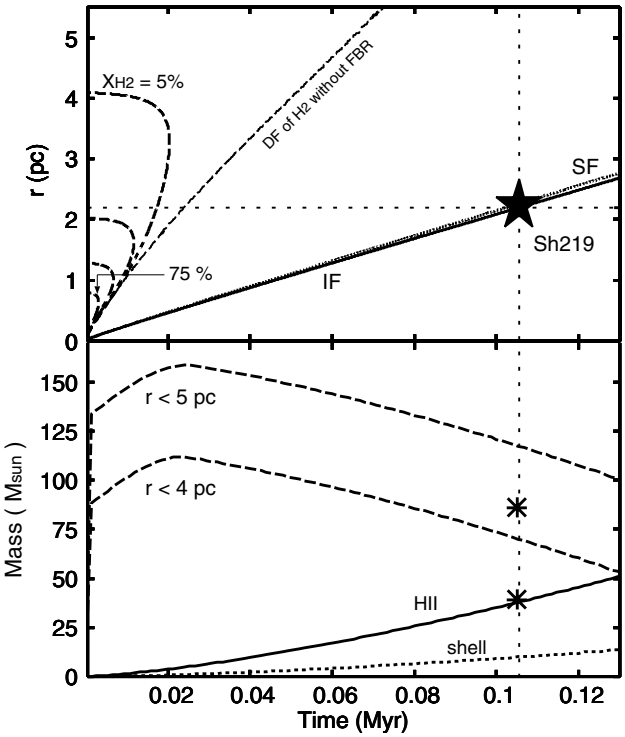

Fig. 8. *Upper panel*: time evolution of the positions of some fronts in our model for Sh219. The solid and dotted line represent the positions of IF and SF. The broken contours denote the positions where the H_2 molecular percentages are 5%, 25%, 50%, and 75% *from top to bottom*. The thin broken line shows the position of the H_2 DF without the FUV background radiation. The horizontal dashed line indicates the observed radius of Sh219, ∼2.2 pc. The H II radius reaches the observed radius at $t \sim 0.105$ Myr, which is indicated with vertical dashed line. *Lower panel*: time evolution of the mass in each region. The solid and dotted lines represent the mass of the ionized hydrogen in the H II region, and neutral hydrogen in the shell respectively. Two broken lines show the mass of the diffuse neutral layer in $r < 4$ and 5 pc. Asterisks indicate the observed mass of the H II region (34 $M_\odot$) and surrounding neutral layer (86 $M_\odot$) by Roger & Leahy (1993).

in the inner 1 pc are photodissociated over the initial 0.01 Myr (see Fig. 6). The upper panel of Fig. 8 presents the time evolution of the chemical structure of the envelope. As this panel shows, H_2 molecules in the envelope completely disappear by the estimated age of Sh219, $t \sim 0.1$ Myr. Almost all H_2 molecules are dissociated by ∼0.04 Myr, and CO molecules in the inner region are destroyed just after the start of the calculation. The H II region is surrounded by the diffuse atomic layer, where the gas temperature is about 300−500 K. Our model suggests that the observed wide neutral layer around Sh219 should not be photon-bounded, but density-bounded. This does not depend on the strength of the FBR. In Fig. 8, we also plot the propagation of the H_2 DF when the FBR is not included. Even without the FBR, FUV photons from the central star easily penetrate into the molecular envelope, and are sufficient for the photodissociation of almost all H_2 molecules in the envelope. This is because the column densities of the shell and envelope are too low to block FUV photons with the steep density gradient of $w = 1.5$ (see Sect. 2).

Figure 8 shows the time evolution of the mass of the H II region and outer neutral layer. Assuming that the neutral layer is density-bounded at $r \sim 4$−5 pc, which is the observed outer radius of the H I layer, the calculated masses at $t \sim 0.1$ Myr, when the IF reaches the observed radius of Sh219, show good agreement with the observed values. The mass of the H I layer, $M_{\rm HI}$, initially increases, because the H_2 molecules in the envelope are photodissociated by the FUV photons from the central star. After all H_2 molecules are destroyed ($t \sim 0.02$ Myr), $M_{\rm HI}$ decreases, because the H II region gradually erodes the H I layer. Note that the mass of the shell is much less than that of the H II region and neutral layer. Most of the swept-up gas does not remain in the shell, but flows into the H II region.

4.2. Timescale of induced star formation

Although Sh219 does not have a clear molecular shell, some observations have suggested that star formation is actually triggered in a molecular cloud present at the periphery of Sh219 (Deharveng et al. 2005, 2006). A young stellar cluster is embedded in the molecular cloud, and elongated along the IF. The cluster includes several massive stars exciting an ultra-compact H II region. One possible triggering scenario is that the IF and the preceding SF enter the pre-existing molecular cloud, and the dense compressed layer forms only in the cloud. The fragmentation of the compressed layer occurs and triggers star formation. Here, we examine this scenario, evaluating the timescale of this triggering process.

The average number density of the molecular cloud is estimated as $n(\mathrm{H_2}) = 8.0 \times 10^3$ cm^{-3} (Deharveng et al. 2006). In our model, the expanding velocity of the IF and SF is 2 $c_{\rm HII} \sim 20$ km s^{-1} ($c_{\rm HII}$ is the sound speed in the HII region). After the IF and SF hit the molecular cloud, the SF can still propagate at ∼several –10 km s^{-1} within the photo-evaporating cloud (Bertoldi 1989). If the cloud size is much smaller than the H II radius, the SF quickly transverses and compresses the cloud. The Mach number of the SF will be of the order of 10, and the density jump at the isothermal SF is

$$\frac{n_2}{n_1} \sim \mathcal{M}^2, \tag{12}$$

where n_1 and n_2 are number densities ahead/behind the SF. With the average cloud number density, the number density just behind the SF can be $n(\mathrm{H_2}) \sim 10^6$ cm^{-3}. The timescale of the fragmentation is,

$$t_{\rm frg} \sim \frac{1}{\sqrt{G\rho}} \sim 8.4 \times 10^4 \ {\rm yr} \left(\frac{n(\mathrm{H_2})}{10^6 \ {\rm cm^{-3}}} \right)^{-1/2}, \tag{13}$$

and $t_{\rm frg}$ with $n(\mathrm{H_2}) \sim 10^6$ cm^{-3} is comparable with the estimated age of Sh219, ∼0.1 Myr. Therefore, triggering is possible. This is also comparable to the typical age of the ultra-compact H II regions (e.g., Wood & Churchwell 1989; Churchwell 2002). Note that if Sh219 is modeled in a homogeneous ambient medium of 30–50 cm^{-3}, the estimated age is much younger, only a few times 10^4 yr (Roger & Leahy 1993). In this case, some special conditions should be satisfied for the rapid triggering scenario: The SF must enter the region that much denser than the average density, and subsequent star (cluster) formation must advance very rapidly.

5. Discussion

5.1. Implication for the feedback effect: negative or positive?

In this subsection, we discuss the role of UV/FUV radiation in star formation in the molecular cloud. Roger & Dewdney (1992) and Diaz-Miller et al. (1998) have calculated the expansion of the H II region and PDR in a homogeneous ambient medium, solving the UV/FUV radiative transfer around a massive star. They have shown that a significant amount of the molecular gas is photodissociated by the FUV radiation. Diaz-Miller et al. (1998) have suggested that the star formation efficiency of the molecular cloud is significantly suppressed by the photodissociation (*negative feedback*). However, our up-to-date calculations, which solve the hydrodynamics as well as the radiative transfer, have shown another aspect of the feedback effect (Papers I and II). We have shown that a dense shell forms, and that most of the swept-up gas remains in the shell in a homogeneous medium. While the FUV radiation destroys the molecular material, FUV photons are shielded by the high column density of the shell. The dense molecular shell forms, where triggering of the subsequent star formation occurs (*positive feedback*). Our quantitative analysis has shown that the positive feedback effect can dominate the negative effect in some cases of a homogeneous medium (Hosokawa & Inutsuka 2006b).

Our current work has shown that the negative feedback effect is promoted only in an inhomogeneous medium. In the cloud with a steep density gradient $w > 1$, the shielding in the shell and envelope becomes inefficient as the H II region expands. The PDR can widely extend around the ionized gas. Consequently, the star formation efficiency will be reduced, though triggering still can occur in the adjacent molecular clouds, as shown in Sh219. Ultimately, the feedback effect by the UV/FUV radiation should be examined in the clumpy, turbulent medium. Some recent studies have calculated the expansion of the H II region in this realistic situation (e.g., Mellema et al. 2006; Mac Low et al. 2006), and suggested that the clumpy structure may also diminish the positive effect (Dale et al. 2005). Although these efforts have not included the outer PDR, similar approaches solving the FUV radiative transfer will make it possible to clarify the role of the FUV radiation. For this purpose, however, the swept-up shell should be resolved with a sufficient number of grids. The column density of the shell often dominates the total column density of the system, which is important for the penetration of FUV photons.

6. Conclusions

We have studied the time evolution of the H II region and surrounding PDR in a radially stratified molecular cloud. We have examined the efficiency of the trapping of FUV photons in clouds with different density profiles represented by $n(r) \propto r^{-w}$, and have focused on the expansion with $w \leq 1.5$. In the molecular cloud with $w > 1.5$, neither the IF nor DFs are trapped, and quickly travel through the whole cloud.

The key physical quantity for the trapping of the FUV radiation is the column density, because the dust absorption is the primary shielding agent. First, we have analytically shown that the time evolution of the column densities of the shell and outer envelope qualitatively switches across $w = 1$. The column density of the shell increases as the H II region expands in the cloud with $w < 1$. When $w > 1$, however, the shell column density decreases, and the column density of the outer envelope quickly decreases as the H II region expands. The quantitative difference across $w = 1$ is significant when the initial column density of the core is several $\times 10^{21}$ cm^{-2}.

Next, we verified the analytic consideration using numerical calculations. The chemical/thermal structure outside the H II region sharply changes with w. In the cloud with a steep density gradient of $w > 1$, the PDR can extend broadly around the H II region. The stellar FUV radiation heats up the envelope to several ×100 K via the photoelectric heating. The trapping of the DFs is sometimes selective. Only CO DF can travel through the whole cloud, while H_2 DF is trapped in the shell. In the steeper density gradient, the trapping of the DFs grows less efficient. If the density gradient is as steep as $w \sim 1.5$, both H_2 and CO DFs quickly propagate in the cloud, and almost all molecules in the envelope are photodissociated. This is contrasted with the expansion in the homogeneous medium and the gradual density gradient of $w < 1$. In these cases, DFs are engulfed by the shell, and the molecular gas gradually accumulates there (Papers I and II).

We have applied this case ($w = 1.5$) to the Galactic H II region, Sh219, whose observational properties are very different from the "collect and collapse"candidates. In Sh219, the ionized gas is not surrounded by a dense molecular shell, but by a diffuse neutral layer. The H II region is denser than the surrounding neutral layer. Our model explains these characteristics of Sh219. The calculated size, density and mass of the H II region and neutral layer are in good agreement with the observed values at $t \sim 0.1$ Myr. We suggest that a density-bounded PDR surrounds the photon-bounded H II region in Sh219.

Acknowledgements. I am grateful to Lise Deharveng for the useful comments and careful reading of the manuscript. I also thank Shu-ichiro Inutsuka for the continuous encouragement and fruitful discussions.

References

Abel, N. P., Ferland, G. J., Shaw, G., & van Hoof, P. A. M. 2005, ApJS, 161, 65
Bertoldi, F. 1989, ApJ, 346, 735
Churchwell, E. 2002, ARA&A, 40, 27
Dale, J. E., Bonnell, I. A., Clarke, C. J., & Bate, M. R. 2005, MNRAS, 358, 219
Deharveng, L., Pena, M., Caplan, J., & Castero, R. 2000, MNRAS, 311, 329
Deharveng, L., Zavagno, A., Salas, L., et al. 2003a, A&A, 399, 1135
Deharveng, L., Lefloch, B., Zavagno, A., et al. 2003b, A&A, 408, L25
Deharveng, L., Zavango, A., & Caplan, J. 2005, A&A, 433, 565
Deharveng, L., Lefloch, B., Massi, F., et al. 2006, A&A, 458, 191
Diaz-Miller, R. I., Franco, J., & Shore, S. N. 1998, ApJ, 501, 192
Elmegreen, B. G., & Lada, C. J., 1977, ApJ, 214, 725
Elmegreen, B. G. 1998, in Origins, ed. C.E. Woodward, M. Shull, & H. A. Thronson, ASP Conf. Ser. (San Francisco: ASP), 150
Ferland, G. J. 2003, ARA&A, 41, 517
Ferland, G. J., Korista, K. T., Verner, D. A., et al. 1998, PASP, 110, 761
Franco, J., Tenorio-Tagle, G., & Bodenheimer, P. 1990, ApJ, 349, 126
Habing, H. J. 1968, Bull. Astron. Inst. Netherlands, 19, 421
Henney, W. J. 2006 [arXiv:astro-ph/0602626]
Hosokawa, T., & Inutsuka, S. 2005, ApJ, 623, 917 (Paper I)
Hosokawa, T., & Inutsuka, S. 2006a, ApJ, 646, 240 (Paper II)
Hosokawa, T., & Inutsuka, S. 2006b, ApJ, 648, L131
Mac Low, M., Toraskar, J., Oishi, J. S., & T. Abel, 2006, ApJ, submitted [arXiv:astro-ph/0605501]
Mellema, G., Arthur, S. J., Henney, W. J., Iliev, I. T., & Shapiro, P. R. 2006, ApJ, 647, 397
Roger, R. S., & Dewdney, P. E. 1992, ApJ, 385, 536
Roger, R. S., & Leahy, D. A. 1993, AJ, 106, 31
Tenorio-Tagle, G. 1979, A&A, 71, 59
Tielens, A. G. G. M., & Hollenbach, D. 1985, ApJ, 291, 722
Wood, D. O. S., & Churchwell, E. 1989, ApJ, 340, 265
Yorke, H. W., 1986, ARA&A, 24, 49
Zavagno, A., Deharveng, L., Comerón, F., et al. 2006, A&A, 446, 171